CHAPTER 3

MODES OR MULTI-LAYERED CIRCULAR RESONATORS

In this Chapter, considered are the 2-D models of multi-layered open dielectric resonators having circular symmetry and partial active regions. The interest to such configurations is caused by the fact that today several leading research groups in the USA (Caltech) and Europe (Zurich Technical University) are engaged in active experimental studies of microdisk lasers placed into annular Bragg reflectors (ABRs), see [83–86, 94, 95].

The goal of this part of the thesis is to study numerically the lasing mode spectra and thresholds for a thin-disk resonator embedded into an ABR and determine the optimal geometrical parameters able to provide lower thresholds of lasing. ABR consists of concentric dielectric rings the space between which is filled in with an optically less dense material or air. In particular, such a reflector can be etched in the substrate and it 2-D model can be built using the effective refractive index technique. The thicknesses of the rings and grooves are usually the same however can be varied, in principle. As the emission from a microdisk laser is taking place predominantly in the disk plane, the presence of ABR gives a hope that the radiation losses can be lowered and therefore the thresholds can be lowered. This is especially important for the lower-index modes.

A microresonator with ABR is an example of an optical circuit composed from several elements where the active region does not coincide with the whole resonator. This is because such a circuit is usually etched or cut by a beam of particles out of a solid wafer containing a quantum well however the pumping is arranged with a narrow pumping beam. The pump beam is always focused on the central disk element in order to avoid the lasing on the ring modes. The simplest configuration of this type is a uniformly active disk in the center of one passive ring, the gap between the disk and the ring being filled in with an optically less dense material or air.

We study the modes in the mentioned resonators numerically, on the basis of rigorous characteristic equations. Besides, we derive the Optical Theorem for the resonators with active regions that enables us to link the mode threshold with its quality factor and the overlap coefficient between the active region and electric field of the given mode. This is especially important for the resonators consisting of several optically coupled regions, only one of which is active.

3.1. Dipole-type supermodes of an active disk in a passive ring

In Fig. 3.1, depicted is a 2-D model of a microdisk laser, concentrically coupled with one passive ring.

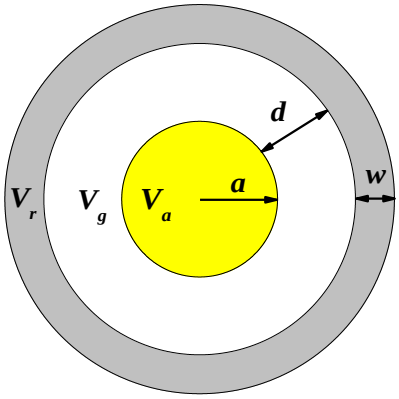

Fig. 3.1 Two-dimensional model of microdisk laser concentrically coupled with a passive ring

Denote the inner disk radius as a and its refractive index as α_a (in the pump-off regime). We will assume that in the pump-on regime the disk becomes uniformly active and has material gain γ (thus, its refractive index becomes complex, $\nu = \alpha_a - i\gamma$), however the ring reflector remains passive. The gap between the disk and the ring has the width d, the ring thickness is w, and the refractive indices of the ring and the gap are α_r andи α_g, respectively. As we are studying the 2-D problem

and imply preceding use of the effective refractive index technique (see subsection 2.1), we will further consider only the case of the H-polarization and understand that the function $U(r,\varphi)$ is the H_z field component.

Thanks to the circular symmetry, the separation of variables enables us to reduce the lasing eigenvalue problem (2.8), (2.12) – (2.13), (2.15) to a transcendental characteristic equation. According to this technique, the field function is represented, in each partial domain, as a series in terms of the trigonometric functions of φ,

$$U^s(\rho,\varphi)=\sum_{m=0}^{\infty}\left[A_m^s J_m(k\nu_s\rho)+B_m^s H_m^{(1)}(k\nu_s\rho)\right]\cos m\varphi, \qquad (3.1)$$

where the index $s=1,\mathrm{K},M+1$ corresponds to the domain number, M is the number of boundaries, and $\left\{A_m^s,B_m^s\right\}$ are unknown coefficients. The numbering of domains starts from the central disk. In the case of simple configuration depicted in Fig. 3.1, M = 3, however we will continue keeping M arbitrary integer and therefore apply the derived equations to more complicated geometries in the next subsections.

Due to the circular symmetry, the modes with different azimuth indices, $m=0,1,2,...$, are orthogonal to each other and can be studies independently. The condition of the local power (2.13) finiteness and the condition at infinity (2.15) lead to conclusion that for each index m the coefficients $B_m^1=0$ and $A_m^{M+1}=0$. On introducing the normalized radii of the ring boundaries as $\rho_1=1$, $\rho_{s>1}=a_{s>1}/a$, where $a_2=a+d$, $a_3=a_2+w$ and substituting (3.1) to the boundary conditions (2.12) on the boundary number s, we obtain a set of two linear equations (for each $m=0,1,2,...$),

$$\begin{aligned}
&A_m^{s+1}J_m(\kappa\nu_{s+1}\rho_s)+B_m^{s+1}H_m^{(1)}(\kappa\nu_{s+1}\rho_s)-A_m^sJ_m(\kappa\nu_s\rho_s)-B_m^sH_m^{(1)}(\kappa\nu_s\rho_s)=0,\\
&\left[A_m^{s+1}J_m'(\kappa\nu_{s+1}\rho_s)+B_m^{s+1}H_m'^{(1)}(\kappa\nu_{s+1}\rho_s)\right]\Big/\nu_{s+1}-\left[A_m^sJ_m'(\kappa\nu_s\rho_s)+B_m^sH_m'^{(1)}(\kappa\nu_s\rho_s)\right]\Big/\nu_s=0,
\end{aligned} \qquad (3.2)$$

where $\nu_1 = \nu = \alpha_a - \gamma, \quad \nu_{2,3} = \alpha_{g,r}$.

After writing (3.2) for all boundaries, $s = 1,...,M$, we obtain a matrix equation f the size $2M \times 2M$. Then the finding of the eigenvalues (κ, γ) is reduced to the search for the roots of the determinantal equation of finite order *2M*,

$$\mathrm{Det}\,\{C_{ij}^{(m)}(\kappa,\gamma)\}_{i,j=1}^{2M} = 0, \quad m = 0,1,2,..., \tag{3.3}$$

where the elements of the matrix operator $C^{(m)}$ are defined by (3.2) for all *s*.

As it has been shown in subsection 2.3, the modes of the lower azimuth indices and, first of all, the monopole modes (m = 0) and the dipole modes (m = 1) in a stand-alone active circular resonator have very high thresholds of lasing because their fields have strong leakage to the outer space. For the modes with the higher azimuth indices *m*, a behavior of the whispering gallery is observed, i.e. their fields are weakly leaky and their thresholds become exponentially small with growing *m*. Therefore it is reasonable to investigate separately the effect of the outer passive rings on the modes with lower and higher azimuth indices *m*. In this subsection, we will present the results of numerical analysis of the dipole-type modes (m = 1) in a circular active resonator inside one passive ring. The whispering gallery modes will be studied in section 3.2.

For the numerical solution of equation (3.3) we have used the secant method. The accuracy of finding the roots has been fixed at the level of 10^{-7}. As initial guesses, we have taken the lasing eigenvalues for an active disk located in free space. The refractive indices were taken as typical values of effective refractive index for a GaAs slab with the 200 nm thickness, $\alpha_a = \alpha_r = 2.63$ and $\alpha_g = 1$ (air), and thus their dispersion was neglected.

In Figs. 3.2 and 3.3, presented are the dependences of the lasing frequencies and thresholds on the normalized distance between the disk and the ring, d/a, for the dipole-type modes $H_{1,n,p,q}$ in the resonator with a thin ring of thickness $w = 0.2a$.

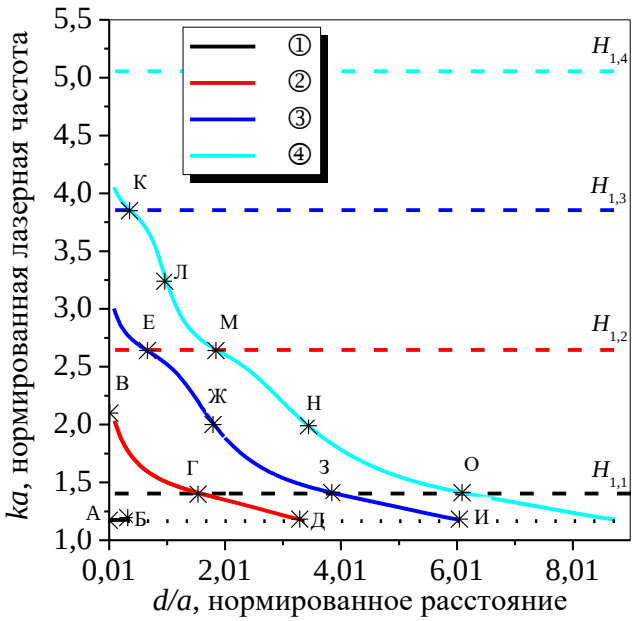

Fig. 3.2 Dependences of the normalized frequencies of supermodes $H_{1,n,p,0}$ (n = 1,2,3,4) on the normalized distance between the active disk and passive ring. The ring thickness is $w = 0.2a$, refractive indices are $\alpha_a = \alpha_r = 2.63, \quad \alpha_g = 1$

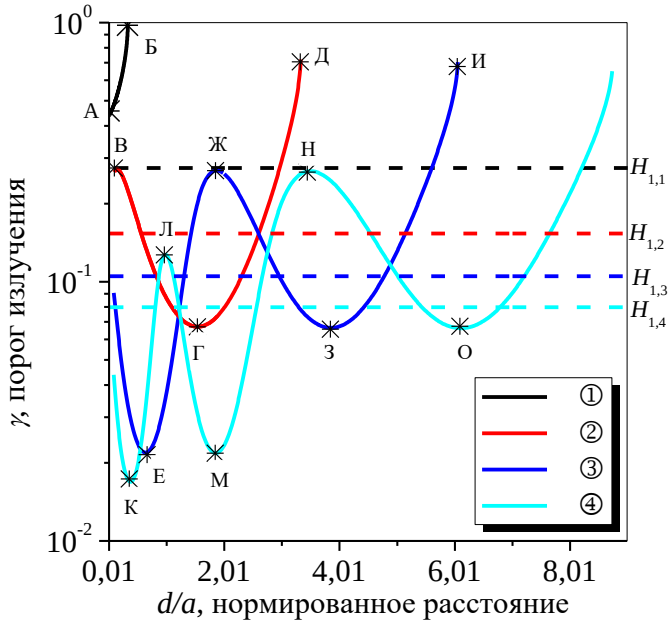

Рис. 3.3 The same as in Fig. 3.2, however for the thresholds of lasing.

Here, the first index (m = 1) gives the number of the field variation in azimuth. The further indices, n, p, and q indicate the numbers of the field variations in radius in each of the partial regions, namely, in the active disk, (passive) air gap, and passive dielectric ring. For the curves in Figs. 3.2 and 3.3, the ring thickness is small and fixed and therefore here $q = 0$. In contrast to the stand-alone resonator, here we have to use several radial indices corresponding to the field variations in each partial region. This reflects the fact that every natural mode of compound resonator is a "supermode", or the mode built from the optically coupled modes of partial regions.

For small values of parameter d (the smallest value was taken as $0.01a$), the curves in Figs. 3.2 and 3.3 marked with numbers from 1 to 4 correspond to the dipole-type modes in the circular resonator of the radius $a + w$ having active region of the radius a in its center. The curve number is also the number of field variations in radius (n = 1,2,3,4, respectively). Horizontal dashed lines present the values of the thresholds and frequencies for the modes $H_{1,n}$ (n = 1,2,3,4) in a stand-alone uniformly active resonator of the radius a with refractive index α_a (see section 2.3). As one can see from the plots, the widening of the air gap between the disk and the ring leads to the monotonic decrement of the frequency of lasing, $\kappa_{1,n,p,0}$ (Fig. 3.2). If the passive ring is taken away from the active disk, the frequencies tend to the value of the dipole mode $H_{1,1}$ in the stand-alone resonator of the radius $a + w$ with active region of the radius a in its center (marked with dotted line).

The change of the distance between the disk and the ring has even greater effect on the thresholds of lasing: they can take the values several times lower and higher than for the same disk in free space. In Fig. 3.3, we show the behavior of the thresholds in dependence of the normalized separation between the disk and the ring.

At any fixed value of the parameter d/a, there are two or even three modes whose frequencies are close to the frequency of the dipole mode $H_{1,1}$ of the stand-alone uniformly active resonator of the radius a (the corresponding eigenvalue in terms of normalized frequency is $\kappa_{1,1} = 1.405$). Note that the mode whose frequency is closest to the mentioned value has always the lowest threshold.

In Fig. 3.4, presented are the patterns of the H-field for the points marked with stars in Figs. 3.2 and 3.3.

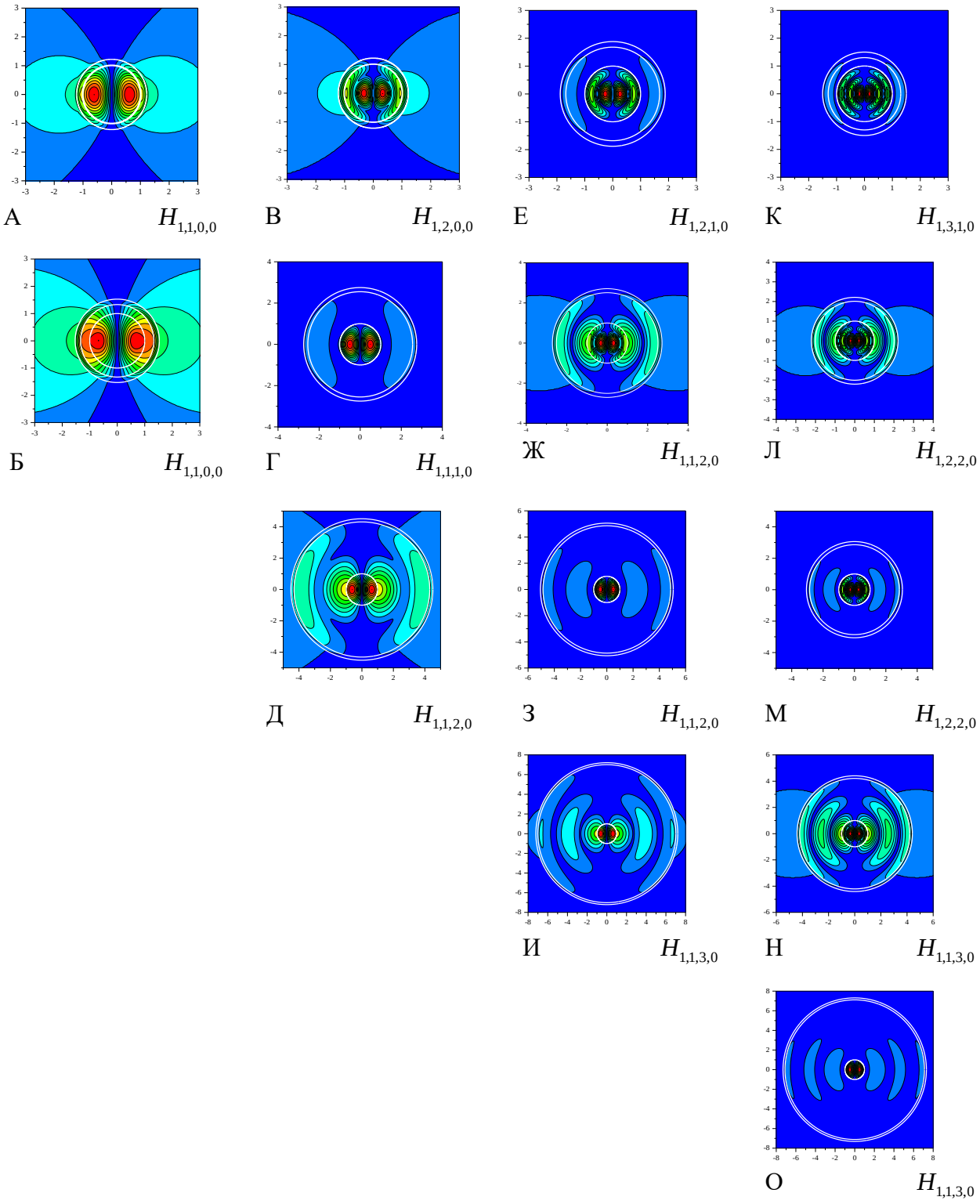

Fig. 3.4 Near-field patterns $|H_z(r,\varphi)|=const$ for the supermodes $H_{1,n,p,0}$, corresponding to parameters marked with stars in Figs 3.2 and 3.3

The locations of the threshold minima and maxima and their limiting values are in agreement with the field-pattern transformations along the structure radius. All points in Figs. 3.2 and 3.3 are marked with capital letters and the corresponding near fields are also marked with the same letters. Inspection of these patterns shows that the modes have the minimum values of thresholds if the intensive spot of the H-field is concentrated in the active region and the leakage to outside is small (see sub-figures Г, Е, З, К, М and О in Fig. 3.4). The maximum thresholds correspond to the situations where the intensive field spot is pushed off the active region to the air gap between the disk and the passive ring (see sub-figures В, Д, Ж, И, Л and Н in Fig. 3.4)) and display an increased field leakage. Removing the ring from the active disk leads to the redistribution of the field inside the compound disk-ring structure that can be characterized with the aid of varying indices *n* and *p*.

Further, numerical study reveals that at the variation of the normalized distance parameter *d/a* all eigenvalues corresponding to the supermodes $H_{1,n,q,0}$ migrate along the same trajectory on the plane (κ,γ) as shown in Fig. 3.5.

Increasing of the gap between the disk and the ring pushes the eigenvalues along this trajectory from the right to the left. However the starting point is different for each dipole-type supermode. These starting points are marked with hollow markers in Fig. 3.5 and coincide with the eigenvalues for the dipole-family modes $H_{1,n}$ in the stand-alone disk of the radius $a+w$ with the active region of the radius *a* in its center. The mentioned above trajectory on the plane (κ,γ) is apparently characteristic for the whole family of dipole modes (with *m* = 1). Its shape depends on the radii and material parameters of ring-like passive regions.

Another type of the mode behavior is observed if the distance between the disk and the ring (i.e. the air gap) is fixed and the passive ring thickness varies. The corresponding to this case dependences of the lasing frequencies and thresholds on the normalized passive-ring thickness w/a are demonstrated in Figs. 3.6 and 3.7.

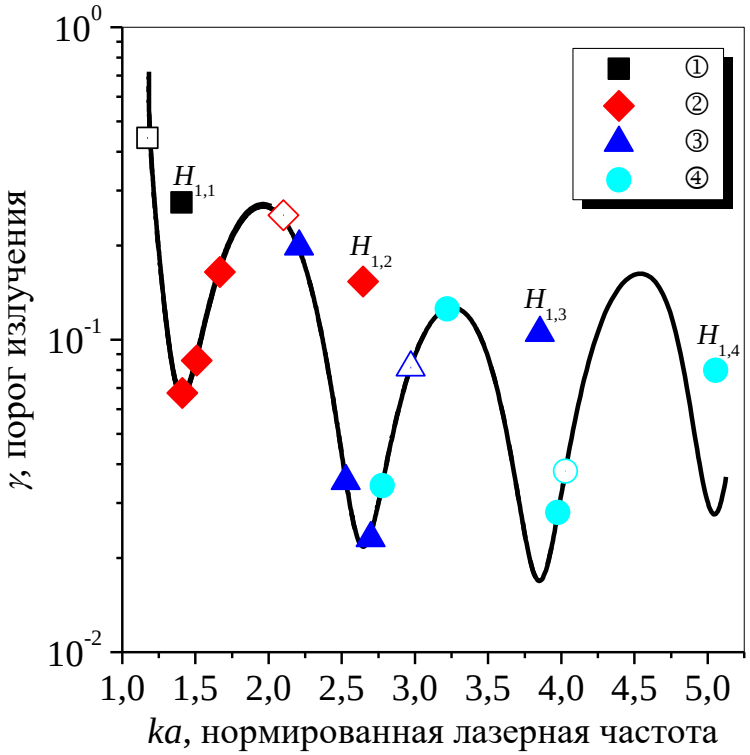

Fig. 3.5 Migration of eigenvalues on the plane (κ, γ) under the variation of *d/a*. Ring thickness is w=0.2a, refractive indices are α_a=α_r=2.63, α_g=1. The mode numbers are the same as in Figs. 3.2 and 3.3. Hollow markers are starting points for the supermodes $H_{1,n,p,0}$ at $d/a = 0.01$. Filled markers correspond to the same eigenvalues at *d/a* = 0.5, 1.0 and 1.5 (from right to left). Off-curve marks are the eigenvalues of the modes of the stand-alone resonator of the radius *a*.

The mode frequencies vary in piece-monotonic manner (Fig. 3.6) and each monotonic section corresponds to the modes having different numbers of the field variations in the passive ring, characterized with the index *q*. As the air gap is narrow, d = 0.5a, the field in it is almost constant and the corresponding index *p* is therefore either 0 or 1. This becomes evident after visualization of the H-field patterns in the marked points (see the markers in Fig. 3.6).

The dependences of the mode thresholds on the normalized ring thickness w/a (Fig. 3.7) demonstrate a number of sharp maxima and deep minima.

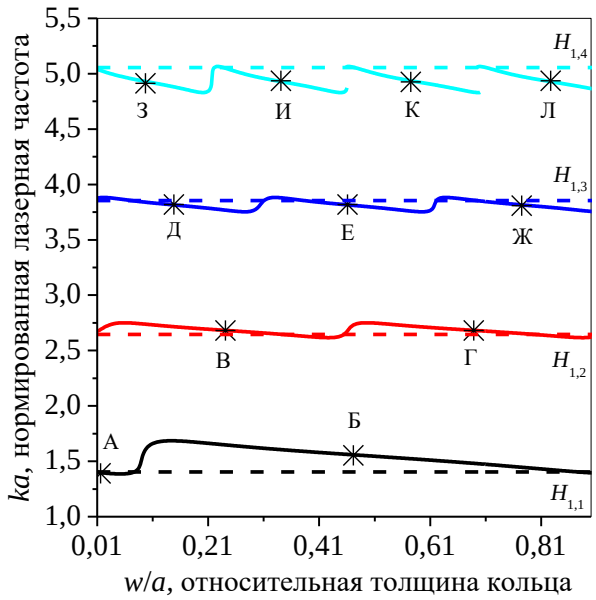

Fig. 3.6 Dependences of the normalized frequencies of the supermodes $H_{1,n,p,q}$ in the active disk embedded in the passive ring on the normalized ring thickness. The air gap thickness is $d = 0.5a$, the refractive indices are $\alpha_a = \alpha_r = 2.63$ and $\alpha_g = 1$.

The minima correspond to the middle points on the monotonic parts of the frequency dependences.

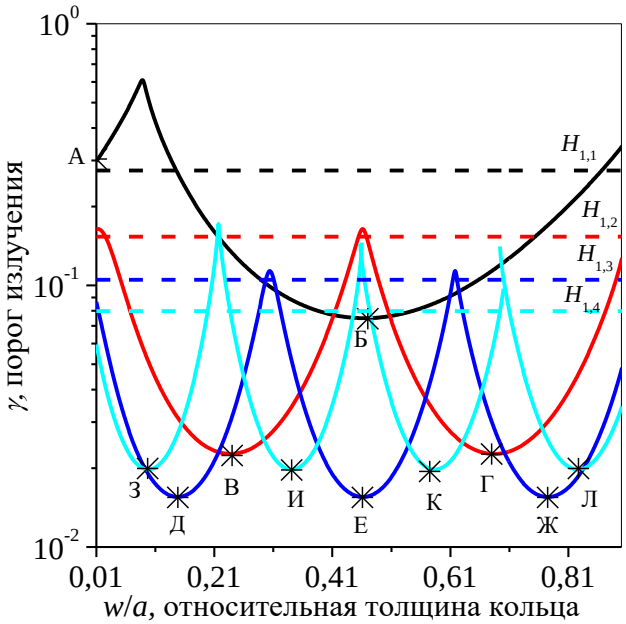

Fig. 3.7 The same as in Fig. 3.6 however for the thresholds of lasing.

The maxima of threshold correspond to the sharp bends where a transformation to the next type of mode takes place (appearance of new field variation in radius in the ring); here the index q takes a value larger by one.

The near-field patterns for the supermodes $H_{1,n,p,q}$ are presented in Fig. 3.8.

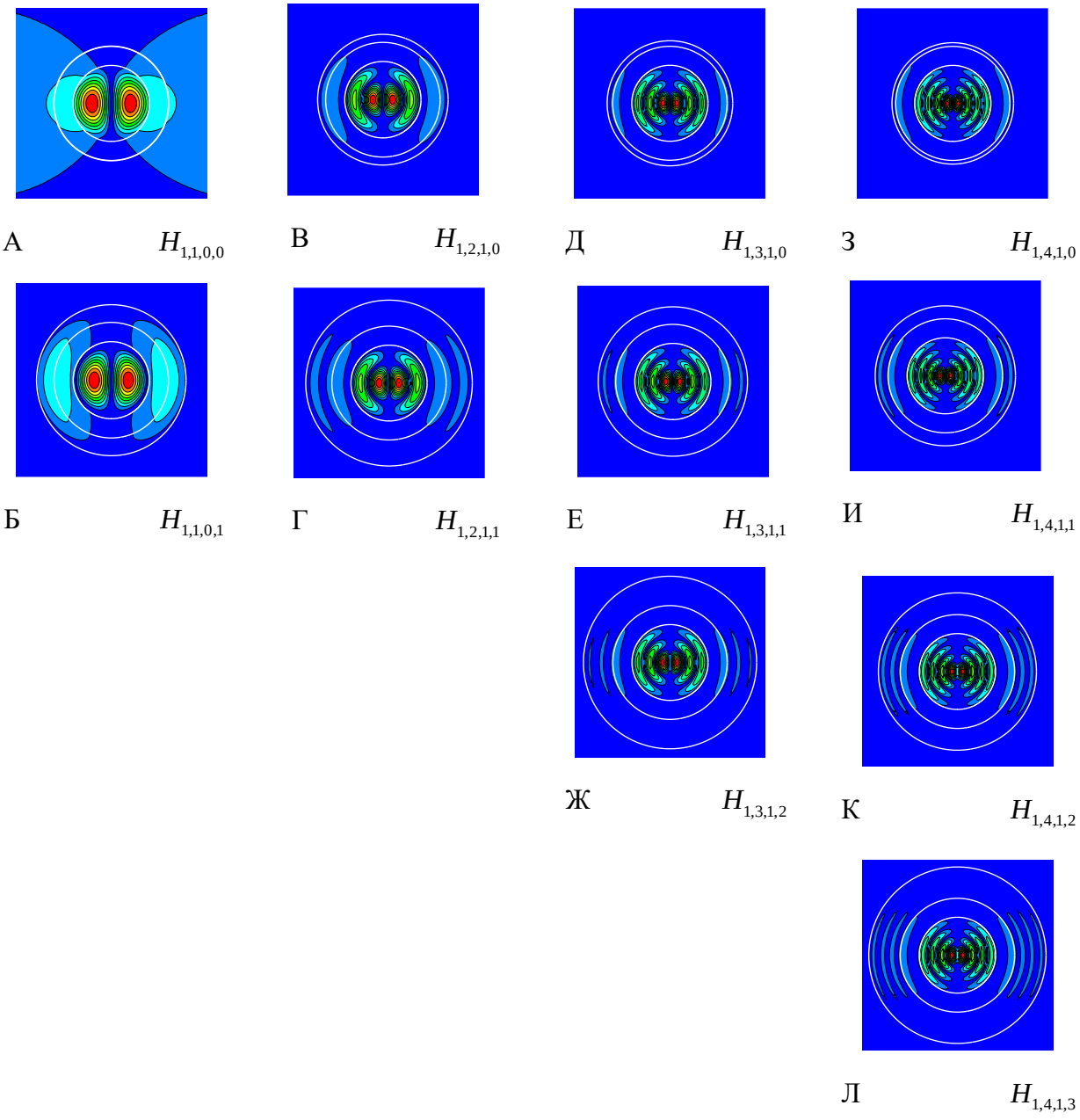

Fig. 3.8 Near-field patterns $|H_z(r,\varphi)|=const$ for the supermodes $H_{1,n,p,q}$ for the points marked with the stars in Figs. 3.6 and 3.7. The distance between the disk and the ring is d=0.5a, the refractive indices are $\alpha_a = \alpha_r = 2.63, \quad \alpha_g = 1$

All modal fields marked with the capital letters form Б to Л in Fig. 3.8 demonstrate high degree of the field concentration in the central active region and weak leakage off the whole structure. In contrast, the field marked with capital letter А demonstrates more significant leakage from the resonator through the passive ring. This is in agreement with the fact that the situation А corresponds to the threshold close to a local maximum (see Fig. 3.7, mark А), while the patterns marked from Б to Л correspond to the minimum values of the mode lasing thresholds (see Fig. 3.7, marks Б to Л). Variation of the passive ring thickness results in appearance of new H-field variation in the ring however the numbers of the field variations in the disk and in the air gap are kept the same (therefore the indices *n* and *p* do not change).

It should be noted that all the mentioned above considerations about the field variations in partial regions (and about the associated indices) are applicable to the supermode electric field as well if one takes account of the fact that the magnetic-field maxima, in the standing wave, always coincide with the electric field zeros, and wise versa.

3.2. Whispering-gallery supermodes of a resonator in an annular Bragg reflector

In this subsection, we will consider the lasing frequencies and thresholds of the supermodes having relatively large values of the azimuth index *m* for a thin active disk embedded into ABR. These modes have low thresholds even in the absence of reflector and they are called the whispering-gallery modes. The aim of the study is the search for the geometrical parameters that provide further lowering of the lasing thresholds.

In Fig. 3.9, depicted is a 2-D model of a microdisk laser with ABR. The central active disk radius is denoted as a and the real-valued refractive index in the pump-off regime is α.

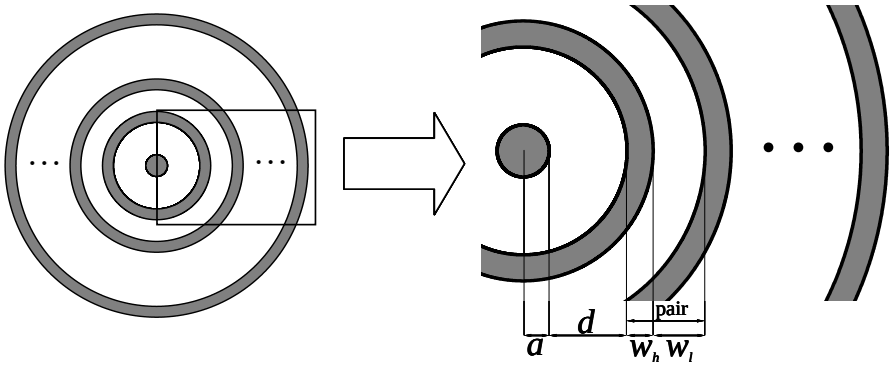

Fig. 3.9 Two-dimensional model of a microdisk laser with ABR

Under pumping, the disk becomes uniformly active and has material gain γ, while the ring reflector remains passive. The distance between the disk and the ring is d. All the rings have the same thickness w_h, and all the grooves have the sum thickness w_l. We will assume that the refractive indices of the rings and grooves are real and denoted as α_h and α_l, respectively, and that $\alpha_h > \alpha_l$.

Using the field representations in each partial region as given by (3.1), we reduce the lasing eigenvalue problem for a disk in ABR to a set of equations like (3.2). Therefore we again obtain a set of independent determinantal equations of finite order (3.3), where $\rho_1 = 1, \quad \rho_2 = 1 + d/a, \quad \rho_{s>2} = a_s / a$ are the normalized radii. Here, $\nu_1 = \alpha - i\gamma$, and if $s = 2,4,...M+1$ (M is an odd number) then $\nu_s = \alpha_l$ and $a_2 = a + d$, $a_{s>2} = a_{s-1} + w_l$, but if $s = 3,5,...M$ then $\nu_s = \alpha_h$ and $a_s = a_{s-1} + w_h$.

In Figs. 3.10 and 3.11, presented are the dependences of the lasing frequencies and thresholds on the normalized distance between the disk and ABR, for the supermode with the azimuth index *m* = 7, that has full notations as $H_{7,1,p,(q)}$. Note that in the absence of ABR this mode has the threshold of $\gamma \approx 10^{-3}$ (see section 2.3).

Every curve in these figures corresponds to the resonator with ABR consisting of 1, 2 or 3 rings. Here we have uses a "compound" index (q), which characterizes the field variations in the rings and grooves of ABR. This is done to shorten the notations, as if we use a separate index for each partial region this will result in a very bulky mode notation.

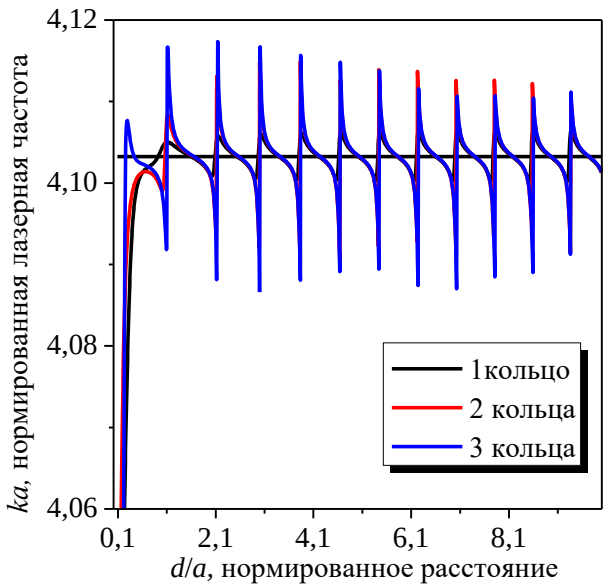

Fig. 3.10 Dependences of the frequencies of supermode $H_{7,1,p,(q)}$ of the active disk in the passive ABR with 1, 2 and 3 rings on the distance between the disk and the first ring of reflector; w_h/w_l=1, w_h=0.2a, α_a=α_h=2.63, α_l=1

Straight lines in the figures show the values of the frequency and threshold of the mode $H_{7,1}$ in the stand-alone active microdisk of the same material.

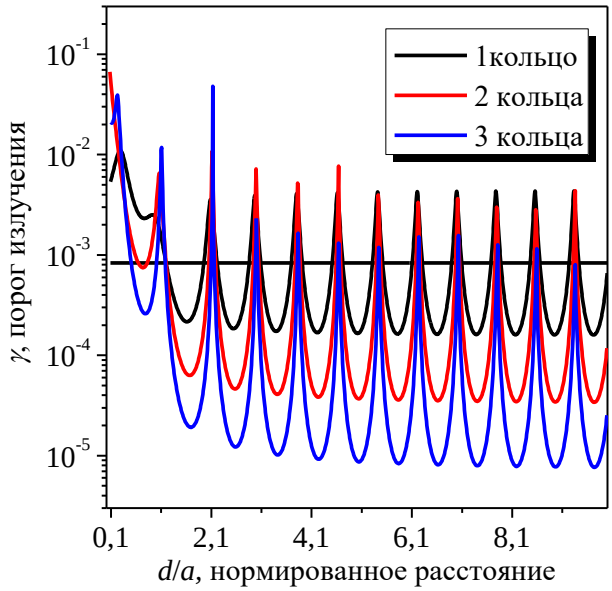

Fig. 3.11 The same as in Fig.3.10, however for the thresholds of supermodes $H_{7,1,p,(q)}$

One can see that if the gap between the disk and the first ring varies the supermode frequency changes only in a fraction of percent (Fig. 3.10). Every monotonic part on the curves corresponds to a separate sub-type of the supermode as here either new filed variations appear in the air gap (then the index p changes) or the field transformation in the ABR rakes place (then the index (q) changes). The field transformation in ABR is explained by the fact that when moving away the reflector from the disk the total radius of the whole structure increases. The variation of thresholds when changing d/a is much more pronounced (Fig. 3.11). Locations of the minima are determined mainly by the ABR period (sum of w_h, and w_l). The depth of the minima is determined by the number of rings (periods) in ABR, and the addition of new ring lowers the threshold of lasing by half-order in magnitude for the optimal distance d/a. If, however, the distance d/a has been chosen not properly, then the lowering of the threshold is not observed.

Further we have studied the effect of the ring thickness w_h on the frequency spectrum and thresholds of lasing for the same supermode – see Figs. 3.12 and 3.13.

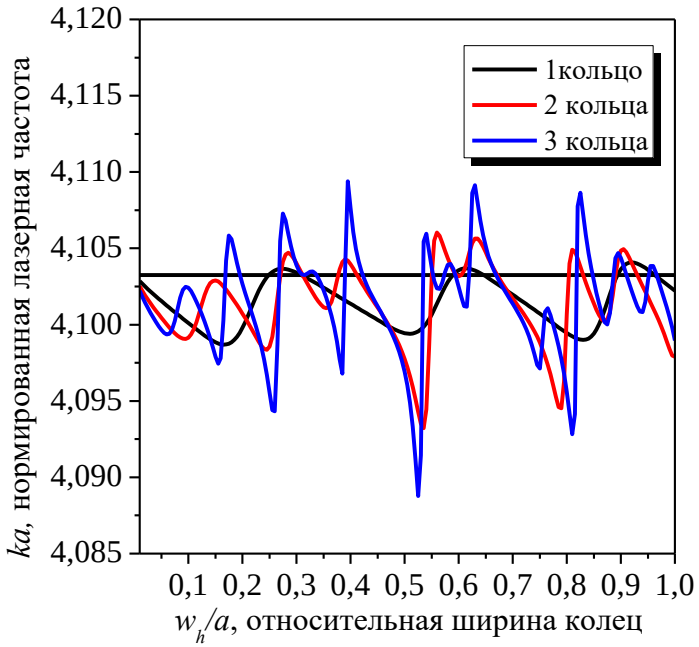

Fig. 3.12 Dependences of the frequencies of supermodes $H_{7,1,p,(q)}$ for the active disk

in a passive ABR with 1,2 and 3 rings (w_h/w_l=1), on the ring thickness; d=0.5a

Here, the rings in the studied ABR have the same refractive index as the disk and the grooves are assumed to be filled with air. The straight lines show the values of the frequency and threshold of lasing for the mode $H_{7,1}$ in the stand-alone resonator with the same parameters. The distance from the disk to the first ring is fixed and equals $d = 0.5a$. For different values of d the results are similar.

In general, the frequencies vary insignificantly when the ring thickness changes. The computed dependences are piece-monotonic and each monotonic part corresponds to a certain supermode $H_{7,1,p,(q)}$.

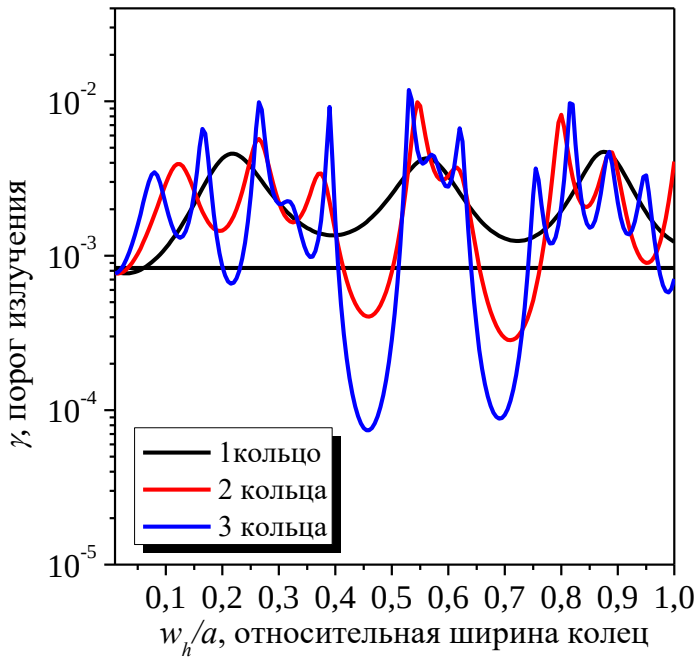

Fig. 3.13. The same as in Fig. 3.12, however for the thresholds of modes $H_{7,1,p,(q)}$

In contrast, the thresholds vary more significantly (Fig. 3.13). One can see the formation of the bands of ring thickness variation where the threshold of lasing gets lower than in the stand-alone active disk. Inside these bands, the lasing thresholds get lower by approximately half-order in magnitude if the number of periods of ABR \is taken larger by one. Note that a similar lowering of thresholds takes place for the

supermodes with other azimuth indices m.

3.3. Optical Theorem for the modes of open resonators

Consider a generic arbitrary-shape 3-D dielectric open resonator with a partial active region, schematically depicted in Fig. 3.14. Here, V_a and V_p denote the active and the passive parts of resonator having boundaries S_a and S_p, respectively, $R_{\min}$ is the radius of the minimum sphere $V_{\min}$, which contains both V_p and V_a. Note that this sphere may contain the free-space part, V_f. We will also imply that the spherical coordinates with a radius-vector $\hat{R} = (R, \varphi, \theta)$ have been introduced, with the origin in the center of the minimum sphere. Suppose also that the outer with respect to the minimum sphere domain is homogeneous and filled with air.

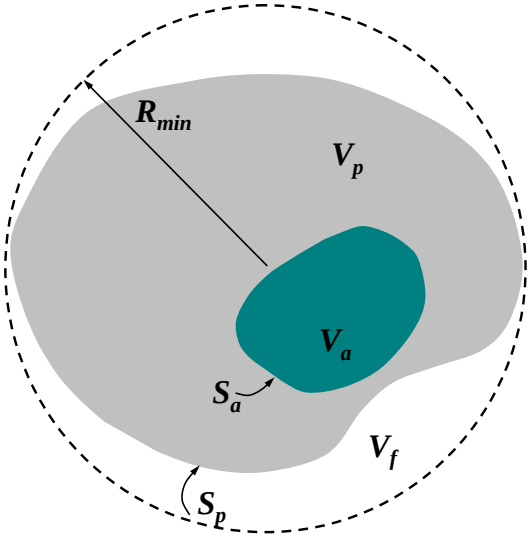

Fig. 3.14 Generic arbitrary-shape resonator with partial active region

The importance of the minimum sphere is in the fact that out of it the electromagnetic field of any natural mode of resonator is expanded in terms of the outgoing to infinity waves only, while inside of it the mode field has the structure of standing wave due to involvement of ingoing waves into field expansions.

A very useful information about the mechanism of light emission from a fully or partially active open resonator can be obtained from the so-called Optical Theorem [54, p. 123] applied to the field of a natural lasing mode, i.e. a solution to the lasing eigenvalue problem (2.8), (2.12) – (2.14). As known, this theorem is an identity that links together the extinction cross-section of a scatterer with the forward-scattered field amplitude for the plane wave incident on a localized obstacle. From the mathematical point of view this identity follows form the vector Green's formula applied to the solution of the time-harmonic Maxwell equations. The most general expression for this identity is also known as the Complex Poynting Theorem. For a complex-valued frequency k the Poynting Theorem has the following form:

$$\Pi = -\frac{1}{2}\int_V (\overset{\mathrm{r}}{j}^{e*}\overset{\mathrm{r}}{E} + \overset{\mathrm{r}}{j}^{m}\overset{\mathrm{r}}{H}^{*})dv + \frac{i}{2}\int_V (k^{*}\varepsilon^{*}Z_0^{-1}\,|\overset{\mathrm{r}}{E}|^2 - k\mu Z_0\,|\overset{\mathrm{r}}{H}|^2)dv, \qquad (3.4)$$

where

$$\Pi = \frac{1}{2}\oint_S \overset{\mathrm{r}}{E}\times\overset{\mathrm{r}}{H}^{*}ds \qquad (3.5)$$

is the full Poynting vector flux through an arbitrary boundary S of a domain V containing all sources and material objects, $\varepsilon = \nu^2$ and μ are the relative dielectric permittivity and magnetic permeability, $\overset{\mathrm{r}}{j}^{e}$ and $\overset{\mathrm{r}}{j}^{m}$ are the given electric and magnetic currents (i.e. the sources), Z_0 is the free-space impedance, and «*» indicates the operation of complex conjugation.

The identity (3.4) can be written for the field of a natural mode as well as a solution to the Maxwell equations in the absence of sources or incident field ($\overset{\mathrm{r}}{j}^{e} = \overset{\mathrm{r}}{j}^{m} = 0$). For a complex natural frequency k_j, (3.4) take the form of

$$(1/2)\oint_S \overset{\mathrm{r}}{E}_j\times\overset{\mathrm{r}}{H}_j^{*}ds = (i/2)\int_V (k_j^{*}\varepsilon^{*}Z_0^{-1}\,|\overset{\mathrm{r}}{E}_j|^2 - k_j\mu Z_0\,|\overset{\mathrm{r}}{H}_j|^2)dv, \qquad (3.6)$$

where the left-hand part is the full Poynting vector flux averaged on the period through the boundary S of the minimum sphere $V_{\min}$ containing all passive and active parts of the open resonator. Here, we use a single cumulative index j for the numbering of the modes, to remind that the complex-frequency spectrum is discrete; the vector function $\{\vec{E}_j, \vec{H}_j\}$ is the electromagnetic field of the j-th mode.

Assume at first that there is no active region in the open resonator, i.e. that $\mathrm{Im}\,\varepsilon \geq 0$ and $\mathrm{Im}\,\mu \geq 0$ everywhere. Extracting the real part from the identity (3.6), we arrive at the familiar expressions,

$$-\mathrm{Re}\,k_j / \mathrm{Im}\,k_j = P_{stored} / (P_{abs} + P_{rad}), \tag{3.7}$$

where the stored, absorbed, and lost for the radiation powers are, respectively,

$$P_{stored} = (1/2)\int_{V_{\min}} (\mathrm{Re}\,\varepsilon Z_0^{-1} |\vec{E}_j|^2 + \mathrm{Re}\,\mu Z_0 |\vec{H}_j|^2) dv, \tag{3.8}$$

$$P_{abs} = (1/2)\int_{V_{\min}} (\mathrm{Im}\,\varepsilon Z_0^{-1} |\vec{E}_j|^2 + \mathrm{Im}\,\mu Z_0 |\vec{H}_j|^2) dv, \tag{3.9}$$

$$P_j^{rad} = \mathrm{Re}\,\Pi_j / \mathrm{Re}\,k_j. \tag{3.10}$$

The formula (3.7) is essentially a definition of the quality factor of the mode of a passive resonator, because $Q_j = -\mathrm{Re}\,k_j / 2\,\mathrm{Im}\,k_j$. Therefore the mode Q-factor in a passive resonator can be calculated either as a ratio of the real to (twice) the imaginary parts of the natural frequency or as a ratio of stored in the resonator power to the power lost for heating and radiation, at the given complex frequency. The both definitions of Q-factor are fully equivalent to each other however the first is simpler to apply provided that k_j has already been found from the characteristic equation.

Further, expression similar to (3.6) can be also derived for the lasing eigenvalue problem, where the frequency is real, $\mathrm{Im}\, k_j = 0$, and $\mathrm{Im}\, \varepsilon < 0$ in the active region, because here $\gamma > 0$. Taking into account that $\varepsilon_a = \nu_j^2 = \alpha^2 - \gamma_j^2 - 2i\alpha\gamma_j$ in the active region and $\mu = 1$, we obtain the Optical Theorem for lasers,

$$\mathrm{Re} \oint_{S_a} \vec{E}_j \times \vec{H}_j^* ds = (2/Z_0)\gamma_j k_j \alpha \int_{V_a} |\vec{E}_j(\vec{R}, k_j, \gamma_j)|^2 dv \qquad (3.11)$$

Thus, the Optical Theorem shows that, for any lasing mode with number j and real frequency k_j, the radiation losses (left-hand part of (3.11)) are compensated by the power generated in the active region V_a (right-hand part of (3.11)) provided that the material gain is γ_j. In other words, this is a rigorous derivation of the classical *Loss = Gain* equation for the mode on the threshold.

It is worth to note that, besides of the real part of (3.6), one can also establish the identity that follows from its imaginary part,

$$2\,\mathrm{Im}\, \Pi_j = k_j \int_V [(\alpha^2 - \gamma_j^2) Z_0^{-1} |\vec{E}_j|^2 - Z_0 |\vec{H}_j|^2] dv\,, \qquad (3.12)$$

where the domain V can be arbitrary. In the limit, if V is a sphere of radius $R \to \infty$, the left-hand part of (3.12) turns zero due to the radiation condition at infinity, (2.5):

$$\Pi = 1/(2Z_0 k_j^{\,2}) \int_0^{2\pi} \int_0^{\pi} [|\Phi^{(1)}(\theta,\varphi)|^2 + |\Phi^{(2)}(\theta,\varphi)|^2] \cos\theta d\theta d\varphi \qquad (3.13)$$

However, the same expression is valid if one shrinks the domain V to the minimum sphere, $V = V_{\min}$, because of the continuity of the Poynting vector flux. Therefore, we obtain that,

$$\int_{V_{\min}} [(\alpha^2 - \gamma_j^{\,2}) Z_0^{-1} |\vec{E}_j|^2 - Z_0 |\vec{H}_j|^2] dv = 0\,, \qquad (3.14)$$

This means that, on resonance, the parts of power related to the electric and magnetic fields inside the open resonator volume, which is its minimum sphere, $V_{\min}$, are equal to each other and the same is valid in the whole space. It should be stressed that this property is valid for both passive and active open resonators.

Now let us give an example of the use of the Optical Theorem in a lasing problem. Consider a 2-D fully active circular resonator of the radius *a* located in free space. The frequencies and thresholds of modes in such a resonator satisfy one of the characteristic equations (2.19) and have been studied in detail in subsection 2.3. Natural-mode fields in this resonator are given by (2.18). The left-hand part of (3.11) for each of polarizations takes the form as

$$\text{E-pol:} \quad \mathrm{Re}\,\Pi_{mn}^{E} = \frac{A^2 2a^2}{Z_0 \pi \kappa_{mn}} \left| \frac{J_m(\kappa_{mn} \nu_{mn})}{H_m(\kappa_{mn})} \right|^2, \tag{3.15}$$

$$\text{H-pol:} \quad \mathrm{Re}\,\Pi_{mn}^{H} = \frac{2Z_0 A^2 a^2}{\pi \kappa_{mn}} \left| \frac{J_m(\kappa_{mn} \nu_{mn})}{H_m(\kappa_{mn})} \right|^2, \tag{3.16}$$

where A is an arbitrary constant and $(\kappa_{mn}, \gamma_{mn})$ are the roots of the characteristic equation (2.19). The right-hand part of (3.11) is, respectively,

$$\text{E-pol:} \quad W_{mn}^{E} = \frac{A^2 a^2}{2Z_0 \gamma_{mn} \kappa_{mn}} \mathrm{Im}[\nu_{mn} \Omega_m^E(\nu_{mn} \kappa_{mn})], \tag{3.17}$$

$$\text{H-pol:} \quad W_{mn}^{H} = \frac{Z_0 A^2 a^2}{2\gamma_{mn} \kappa_{mn}} \mathrm{Im}[\nu_{mn} \Omega_m^H(\nu_{mn} \kappa_{mn})], \tag{3.18}$$

where

$$\Omega_m^E(x) = J_{m-1}(x) J_m(x^*), \qquad \Omega_m^H(x) = J_{m-2}(x) J_{m-1}(x^*) + J_m(x) J_{m+1}(x^*) \tag{3.19}$$

Наконец, теорема Пойнтинга (3.11) для активного круглого резонатора в свободном пространстве принимает вид:

$$\alpha \operatorname{Im}\Omega_m^{E,H}(\kappa_{mn}\nu_{mn}) - \gamma \operatorname{Re}\Omega_m^{E,H}(\kappa_{mn}\nu_{mn}) = \frac{2\alpha}{\pi\kappa_{mn}}\left|\frac{J_m(\kappa_{mn}\nu_{mn})}{H_m(\kappa_{mn})}\right|^2, \qquad (3.20)$$

The computations show that the identity (3.20) is satisfied with a higher accuracy (usually with machine precision) than the accuracy of finding the eigenvalue elements κ_{mn} and γ_{mn} from corresponding characteristic equation.

From the other side, taking into account that for the fully active open circular resonator $V_a = V_{\min}$ and using notation (3.10), one can re-write identity (3.11) as

$$\gamma_j = \frac{\alpha \operatorname{Re} \Pi_j(k_j,\gamma_j)}{k_j W_j(k_j,\gamma_j)} = \frac{\alpha P_j^{rad}}{W_j(k_j,\gamma_j)} \qquad (3.21)$$

where

$$W_j(k_j,\gamma_j) = (A^2/Z_0)\int_{V_{\min}} \alpha^2 |\vec{E}_j(\vec{R},k_j,\gamma_j)|^2 dv, \qquad (3.22)$$

If, additionally, we assume that the mode electric field is normalized to its maximum-magnitude value, i.e. $A = A_j = \max^{-1}|\vec{E}(\vec{R},k_j,\gamma_j)|$, then (3.22) coincides with the quantity playing remarkable role in the Cavity Quantum Electrodynamics (CQED) and is called the *effective mode volume*. However, in CQED this quantity is usually introduced from heuristic considerations, differs in different publications (commonly the integration involves the domain occupied with dielectric only, i.e. not $V_{\min}$), and is assumed to be the same for passive and active resonators [159]. In contrast to this, we have come to the effective mode volume using only the mathematical manipulations with Maxwell equations, i.e. from first principles.

The quantity standing in the right-hand part of (3.21) is, up to the constant α, the ratio of the radiated to the stored (averagely on the period) powers in the

resonator, P_j^{rad}/W_j. Thus, it is the inverse value of what is usually called the mode Q-factor. To emphasize the fact that here we deal with an active resonator we will use the notation $\tilde{Q}_j$ for this quantity. Therefore the threshold of lasing of any mode in fully active resonator is inverse proportional to its quality-factor,

$$\gamma_j = = \frac{\alpha}{\tilde{Q}_j} \tag{3.23}$$

Note that when calculating the active-cavity Q-factor, $\tilde{Q}_j$, one can neglect the presence of gain $\gamma_j \neq 0$ and replace $\tilde{Q}_j$ with the counterpart value for the passive resonator, Q_j (see the comments after equation (3.7)). The error of such a replacement has the order of $O(\gamma_j^2)$ and therefore is small for the modes having low thresholds.

3.4. Overlap coefficients between the active region and the mode field

More interesting is a configuration where the active region is only a part of the whole volume of open resonator, i.e. of the corresponding minimum sphere. For instance, this can be an active disk concentrically coupled with a passive ring shown in Fig. 3.1, where $V_{\min}$ contains active circle, air gap, and passive ring. In this case for every *j*-the mode it is convenient to write the effective mode volume as

$$W_j(k_j,\gamma_j) = \frac{1}{Z_0}\int_{V_{\min}} \alpha^2 \,|\, \vec{E}_j(\vec{R},k_j,\gamma_j)\,|^2 dv = W_j^{(a)} + W_j^{(p)} + W_j^{(f)}, \tag{3.24}$$

where the partial mode volumes and the corresponding overlap coefficients are

$$W_j^{(s)}(k_j,\gamma_j)=\frac{1}{Z_0}\int_{V_f}\alpha_f^2\,|\,\vec{E}_j(\vec{R},k_j,\gamma_j)|^2dv,\quad \Gamma_j^{(s)}=W_j^{(s)}/W_j,\quad s=a,p,f \qquad (3.25)$$

Each overlap coefficient shows the fraction of electric-field power of the *j*-th mode that is contained in the given active of passive partial region of resonator. Note also that from (3.24) it follows that $\Gamma_j^{(a)}+\Gamma_j^{(p)}+\Gamma_j^{(f)}=1$. It is important to remember that all these quantities have sense only on resonance, i.e. at the discrete values of frequency and threshold associated with certain lasing mode. Now the Optical Theorem (3.11) can be re-written as follows:

$$\gamma_j=\frac{Z_0\,\mathrm{Re}\oint_{S_a}\vec{E}_j\times\vec{H}_j^{*}ds}{2k_j\alpha_a\int_{V_a}|\,\vec{E}_j(\vec{R},k_j,\gamma_j)|^2dv}=\frac{\alpha_a P_j^{rad}}{\Gamma_j^{(a)}W_j}, \qquad (3.26)$$

where P_j^{rad} is the total power flux radiated by the given mode into the outer space. All quantities in the right-hand part of (3.26) indirectly depend on the material gain γ_j via Maxwell equations. The quantity P_j^{rad}/W_j in the right-hand part of (3.26) is again the ratio of the radiated to the stored powers in the resonator. This is inverse value to the Q-factor of open resonator with active region and therefore,

$$\gamma_j=\frac{\alpha_a}{\Gamma_j^{(a)}\tilde{Q}_j}. \qquad (3.27)$$

Equation (3.27) is very simple however contains very important message. As noted earlier, if the mode threshold is low, $\gamma<<1$, then $\tilde{Q}_j\approx Q_j$ with an error of $O(\gamma^2)$. Therefore (3.27) shows that a high Q-factor in the pump-off regime is not a sufficient condition for obtaining a low threshold in the pump-on regime. Equally important is the value of the overlap coefficient of the active region with the electric field of the given mode.

Note also that in the case of the fully active cavity $\Gamma_j^{(a)} \equiv 1$, and (3.27) turns to (3.23). Let us give the examples of partially active resonators.

The first example is a circular resonator with radially non-homogeneous active region considered in subsection 2.4. We remind that here the active region is either a circle of a smaller radius $b\,(b<a)$ or a ring adjacent to the resonator rim with the inner radius b. In the active region, we assume a constant gain, $\nu = \alpha - i\gamma$. The corresponding mode frequencies and thresholds have been studied in subsection 2.4.

The effective mode volume is introduced here via expressions (3.24) with account of only two partial domains, V_a and V_p (active and passive parts) and the overlap coefficients for the *j*-the mode are two, $\Gamma_j^{(a)}$ and $\Gamma_j^{(p)}$. Note that $\Gamma_j^{(a)} + \Gamma_j^{(p)} = 1$ because $V_{\min} = V_a + V_p$, and hence it is enough to determine numerically only one overlap coefficient. The Q-factor of the resonator with a partial active region and the threshold of the same mode are linked together via identity (3.27).

The computation of the overlap coefficients needs integration of the products of cylindrical functions and their derivatives of the same integer index *m* (see subsection 3.1). Using the field representation from (3.1) and the definition of $W_j^{(s)}$ from (3.25), in each partial region one has to take the following integrals:

$$W_j^s = \frac{1}{Z_0}\int_{V_s} \alpha^2 |E|^2 \,\rho d\rho d\varphi =$$

$$\frac{\pi\alpha^2 Z_0^2}{2\nu_s \nu_s^*}\int_{a_s}^{a_{s+1}} [|A_m^s|^2 (J_{m-1}J_{m-1}^* + J_{m+1}J_{m+1}^*) + A_m^s B_m^{s\,*}(J_{m-1}H_{m-1}^{(1)*} + J_{m+1}H_{m+1}^{(1)*}) + \qquad (3.28)$$

$$A_m^{s*} B_m^s (J_{m-1}^* H_{m-1}^{(1)} + J_{m+1}^* H_{m+1}^{(1)}) + |B_m^s|^2 (H_{m-1}^{(1)} H_{m-1}^{(1)*} + H_{m+1}^{(1)} H_{m+1}^{(1)*})]\rho d\rho,$$

where s is the index of the integration domain. The argument of the cylindrical functions in (3.28) is $\kappa\nu_s\rho$. Depending on whether active or passive is the domain of integration one has to take integrals of the products of functions with either complex-

conjugate arguments or the same real. According to that consideration, the following formulas are applied [160]:

$$\int Z_m(\kappa\nu\rho)T_m(\kappa\nu^*\rho)\rho d\rho = \frac{\rho}{\kappa}\left[\frac{\nu^* Z_m(\kappa\nu\rho)T^*_{m-1}(\kappa\nu\rho) - \nu Z^*_{m-1}(\kappa\nu\rho)T_m(\kappa\nu\rho)}{\nu^2 - \nu^{*2}}\right] \quad (3.29)$$

and

$$\int Z_m(\kappa\alpha\rho)T_m(\kappa\alpha\rho)\rho d\rho = \frac{\rho^2}{4}[2Z_m(\kappa\alpha\rho)T_m(\kappa\alpha\rho) - Z_{m-1}(\kappa\alpha\rho)T_{m+1}(\kappa\alpha\rho) - Z_{m+1}(\kappa\alpha\rho)T_{m-1}(\kappa\alpha\rho)], \quad (3.30)$$

where $Z_m(\cdot)$ and $T_m(\cdot)$ are arbitrary cylindrical functions of integer order.

Using (3.29), we obtain that $W^{(a)}_{mn}$ is computed after formula (3.18). The power of electric field contained in passive regions is computed after (3.28) with the aid of (3.30) and has as many as 16 terms (after substituting the corresponding limits of integration).

In Figs. 3.15 – 3.17, presented are the numerical results computed for the whispering-gallery modes $H_{7,n}$ ($n = 1,2,3$ is the number of the field variations in radius), without account of the effective refractive index dispersion, so that $\alpha_{eff} = 2.63$ (this is unlike subsection 2.4, where we took dispersion into account).

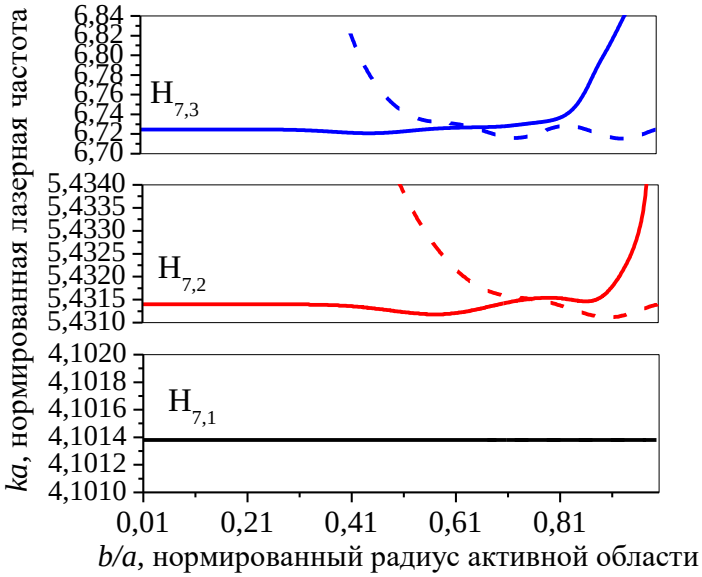

Fig. 3.15 Dependences of the lasing frequencies and thresholds of the modes $H_{7,n}$, $n=1,2,3$ on the relative radius of the active region in the disk laser. Solid curves are for the resonator with a ring-like active region and dashed curves are for the active circle of smaller radius. $\alpha_{eff}=2.63$

In this case we have used only one index, n, for the characterization of the field variations in radius, despite the presence of two partial regions. This is because the refractive indices differ by a small value γ that is present in the active region ($\nu_a=\alpha_{eff}-i\gamma$). Two types of curves in Figs. 3.15 and 3.16 demonstrate the dynamics of the behavior of the lasing frequencies and thresholds in the same open circular resonator with two types of active regions: in the shape of the circle of smaller radius *b* and in the shape of a ring with the inner radius *b*. As one can see, if radius *b* varies, the curves of the thresholds corresponding to these two types of active regions cross each other at some value of *b/a* (see Fig. 3.16). The behavior of the corresponding overlap coefficients of active region is shown in Fig. 3.17.

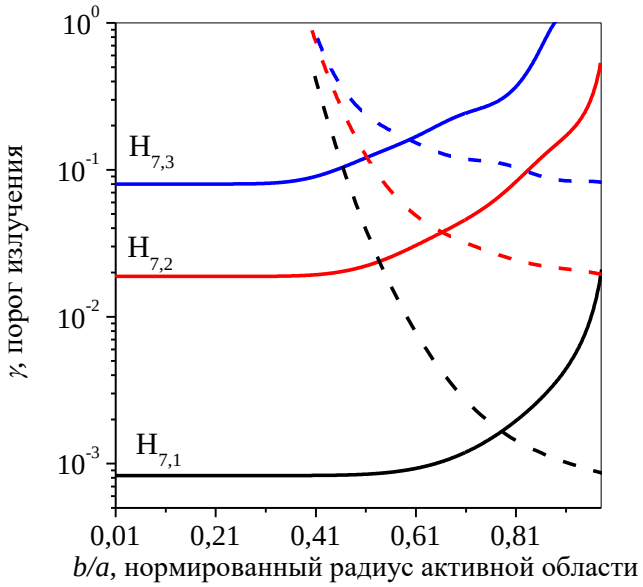

Fig. 3.16 The same as in Fig. 3.15, however for the thresholds of lasing

What is remarkable, at the point of crossing the threshold of the whispering-gallery modes is twice higher, up to several digits, than for the same mode in a uniformly active circular resonator. This effect can be explained with the aid of the Optical Theorem. Indeed, in this case the contrast between the refractive indices of the active and passive regions is small, of the order of $O(\gamma)$.

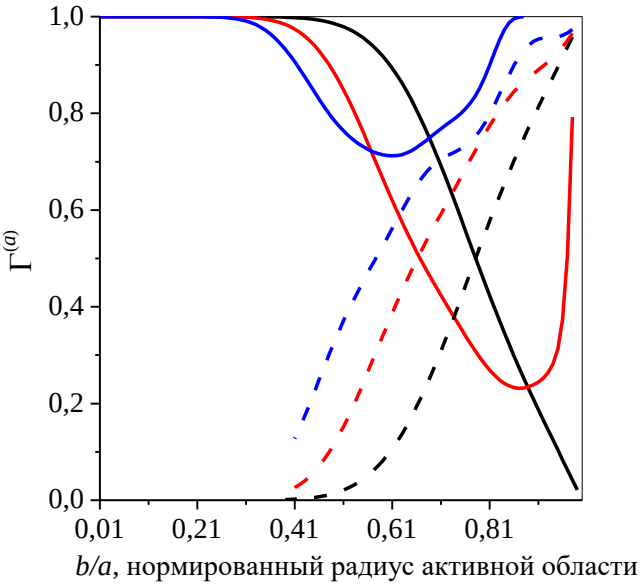

Fig. 3.17 The same as in Fig. 3.15, however for the overlap coefficient of the active region

Besides, the frequency of the whispering-gallery mode and its field also differ within this estimate. Therefore the mode Q-factors in the active and passive cavities with of same radius and material differ by $O(\gamma^2)$. Then, the Optical Theorem tells that the growth in threshold in two times can be explained only by a drop in the active-region overlap coefficient to the value of $\Gamma_{7,n}^{(a)} = 1/2 \quad (n = 1,2,3)$. To verify this explanation, we have computed these coefficients as a function of *b/a* . The plots in Fig 3.17 fully support our understanding of the mechanism behind the behavior of the mode thresholds. We do not show the overlap coefficients of the passive region because $\Gamma_{7,n}^{(p)} = 1 - \Gamma_{7,n}^{(a)} \quad (n = 1,2,3)$.

As a second example, consider an active circle concentrically coupled with a passive ring (see Fig. 3.1.) whose mode frequencies and thresholds of lasing have been studied in subsection 3.1. Here the minimum sphere is the circle of the radius $a + d + w$, the active region V_a is the circle of the radius a, and two passive regions V_g and V_r are the air-filled and dielectric-filled rings of corresponding radii. The mode effective volume and overlap coefficients are defined by (3.24) - (3.25).

The numerical results obtained for the dipole-type supermodes of the active disk coupled with a passive ring are shown in Figs. 3.18 – 3.20.

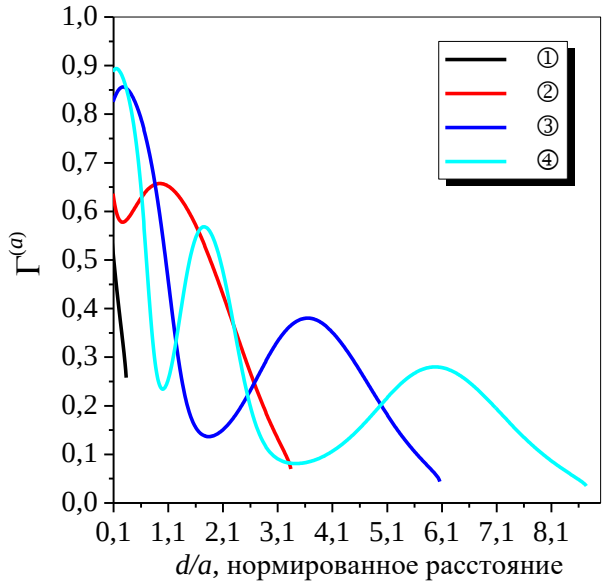

Fig. 3.18 Overlap coefficients of the active region with the fields of supermodes $H_{1,n,p,0}$ (n =1,2,3,4) for the active disk in the passive ring as a function of the distance from the disk to the ring. The parameters of the resonator are the same as in Fig. 3.3

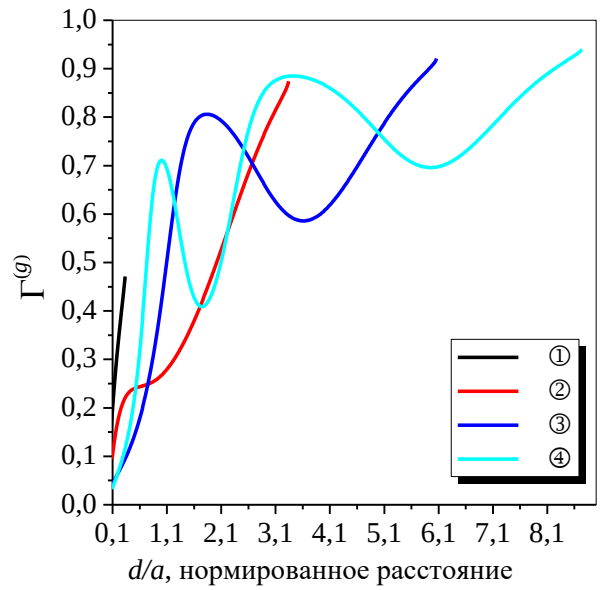

Fig. 3.19 The same as in Fig. 3.18, however for the overlap coefficient of the air gap.

Overlap coefficients for the electric field of the dipole-type supermodes $H_{1,n,p,0}$ (n = 1,2,3,4) with each of the partial regions (active disk, ring-like air gap, and

passive dielectric ring) are plotted in dependence of the normalized distance d/a and correspond to the plots in Fig. 3.3.

As one can see from a comparison with Fig. 3.3 of subsection 3.1, the overlap coefficients of the active region, $\Gamma^{(a)}_{1,n,p,0}$ (Fig. 3.18), indeed behave like inverse values of the mode thresholds (accounting for the logarithmic scale for the thresholds in Fig. 3.3). In contrast, the overlap coefficients of the air gap, $\Gamma^{(g)}_{1,n,p,0}$ (Fig. 3.19), almost copy the variation of the thresholds for the studied here dipole-type supermodes. As for the third partial region, the overlap coefficients of the passive dielectric ring, $\Gamma^{(r)}_{1,n,p,0}$, keep almost uniformly small values around 0.03 (Fig. 3.20). An exception is the situation where a passive ring is located very close to the active disk.

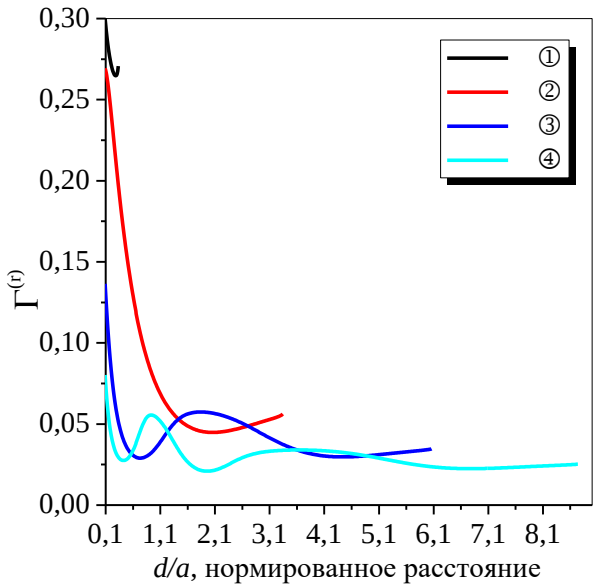

Fig. 3.20 The same as in Fig. 3.18, however for the overlap coefficient of the passive dielectric ring

This behavior is explained by the small thickness of the passive ring in this numerical example ($w = 0.2a$, or $w < \lambda/\alpha$, where λ is the wavelength).

Thus, we may conclude that if the thickness of the passive dielectric ring is small, then the low modal thresholds of lasing are observed for the mode electric field is pulled into the active region. Correspondingly, the high thresholds are found if the

mode field is pushed out of the active region and pulled into the air gap between the active disk and passive ring.

In the vase of a thicker ring, the mode field may be also partially pulled into the ring. Therefore the dynamics of the variation of thresholds in Fig. 3.3 is explained by the field re-distribution between three partial regions (active circle, passive ring-like air gap and passive dielectric ring). The sharp bends on the dependences of thresholds on the ring thickness (Fig. 3.7) are always caused by the formation of new variation of the electric field where the "ring" index q get larger by a unite. All these variations are in mutual agreement as suggested by (3.27).

Finally, consider a third example which is an active circular resonator with ABR (see subsection 3.2). The mode effective volume and the overlap coefficients are again given by (3.24) – (3.25). As ABR contains many (M-1) partial domains, it is convenient here to introduce not $M-1$, but only two partial mode volumes. Namely, the partial mode volume over the dielectric regions, $W_j^{(r)}$ (the air gap regions, $W_j^{(g)}$), is the sum of integrals taken over dielectric (air-gap) rings only. Then the total effective mode volume is $W_j = W_j^{(a)} + W_j^{(r)} + W_j^{(g)}$, where $W_j^{(a)}$ is the mode volume of the active region. The overlap coefficients of the partial regions are introduced after (3.25). For the circular and ring-like domains, the mode volumes are calculated after (3.28) – (3.30).

Numerical results obtained for the overlap coefficients of the whispering-gallery supermodes $H_{7,1,p,(q)}$ are presented in Figs. 3.21 – 3.26. One can see their behavior at the same variations of the ABR parameters as in section 3.2, where the lasing frequencies and thresholds have been studied. A comparison with Fig. 3.11 shows that if the distance d/a varies, then the overlap coefficients of the active region, $\Gamma_{7,1,p,(q)}^{(a)}$ (Fig. 3.21), vary in inverse ratio to the mode thresholds, and their maxima do not exceed 0.82.

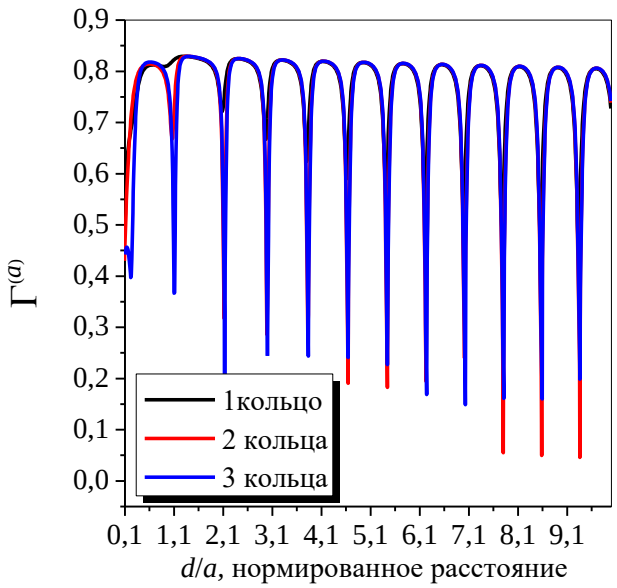

Fig. 3.21 Overlap coefficients of the active region for the supermode $H_{7,1,p,(q)}$ in a resonator with ABR as a function of distance *d/a*. Other parameters as in Fig. 3.10

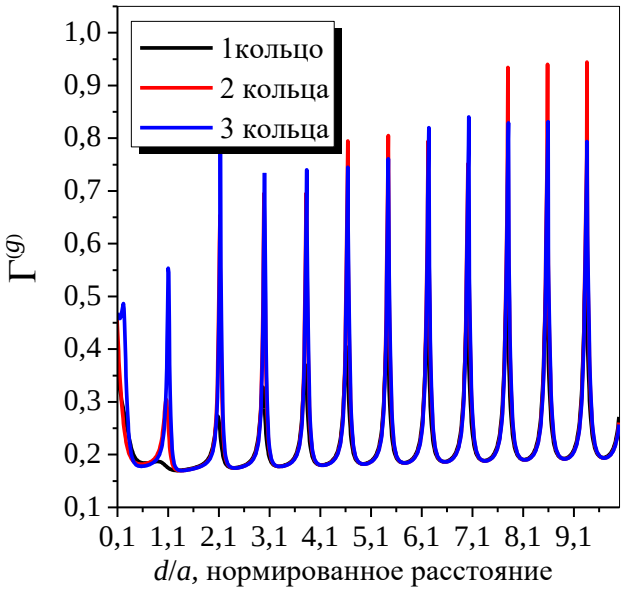

Fig. 3.22 The same as in Fig. 3.21, however for the summary overlap coefficient for the air gaps.

The overlap coefficients for the air-gap rings, $\Gamma^{(g)}_{7,1,p,(q)}$ (Fig. 3.22), do not drop lower then 0.18 and almost copy the behavior of the thresholds of the studied

supermodes in the resonator with ABR. Here, the growth of these coefficients take place mainly at the expense of periodic concentration of the mode electric field in the region with the number $s=2$, i.e. in the air gap between the active region and the first dielectric ring.

As about the passive dielectric rings, their summary overlap coefficient, $\Gamma^{(r)}_{7,1,p,(q)}$, has low values around 0.01 almost everywhere (Fig. 3.23) except of the domain $d/a<0.2$ that can be explained by small thickness of the rings.

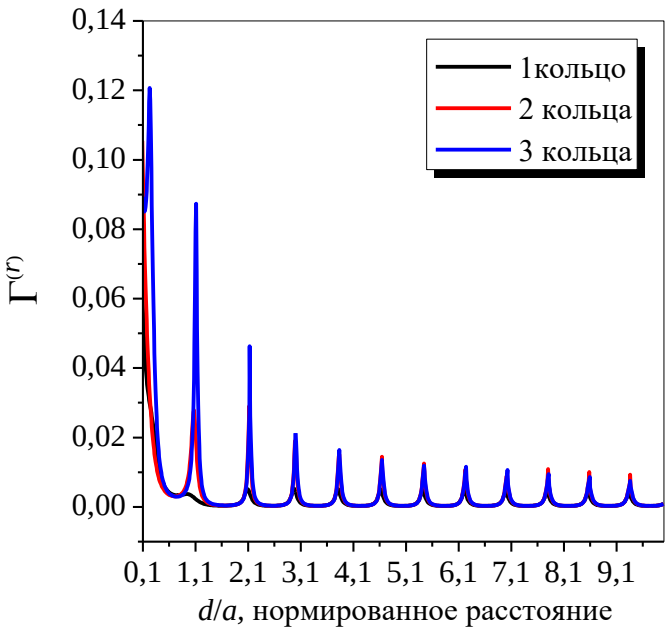

Fig. 3.23 The same as in Fig. 3.21, however for the summary overlap coefficient of the passive dielectric rings

Thus, one can conclude that if the period of the passive dielectric ABR is small, then the low lasing thresholds are observed for the mode electric field pulled into the active region in the center of resonator. The high thresholds are found for the m0de field pushed out of the active region and concentrated in the air gap between the active disk and the first ring of ABR.

In Figs. 3.24 – 3.26, shown are the dependences of the overlap coefficient of the active region and the summary overlap coefficients of the passive dielectric rings

and the air-gap rings of ABR on the normalized thickness of rings, for the whispering-gallery supermodes $H_{7,1,p,(q)}$. The parameters of the studied resonators are the same as used in subsection 3.2 when studying the lasing frequencies and thresholds of the same supermodes; in particular, here $w_h = w_l$.

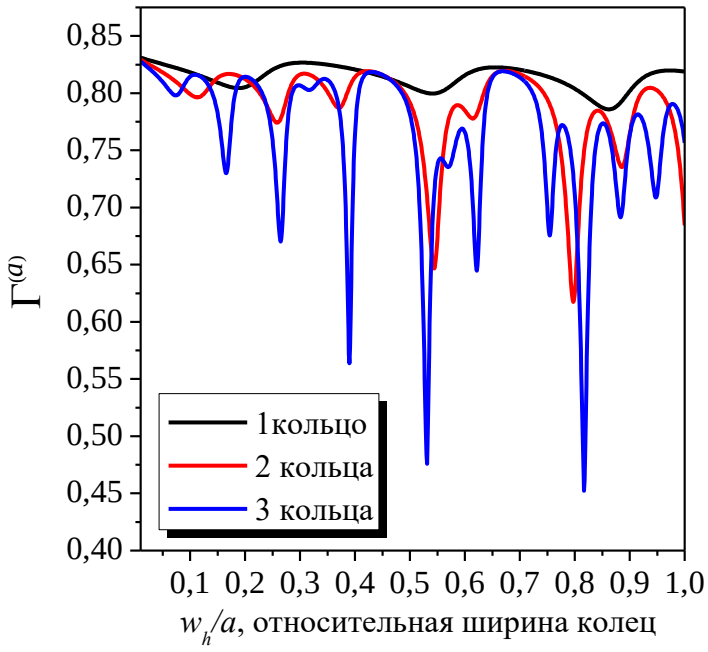

Рис. 3.24 Overlap coefficients of the active region for the supermode $H_{7,1,p,(q)}$ in dependence of the ABR ring thickness. Other parameters are the same as in Fig. 3.12

As before, the overlap coefficients of the active region, $\Gamma^{(a)}_{7,1,p,(q)}$, vary approximately as inverse ratio of the corresponding thresholds (compare to Fig. 3.13). At the same time, they do not exceed 0.83. The main difference from the previous numerical examples is the fact that each of the two summary overlap coefficients, over the passive dielectric rings, $\Gamma^{(r)}_{7,1,p,(q)}$, and over the air gaps, $\Gamma^{(g)}_{7,1,p,(q)}$, is able to take relatively large values, up to 0.35 and 0.20, respectively, at certain values of the ring thickness w_h / a. This is because the thicknesses of the rings and air gaps are comparable to the wavelength.

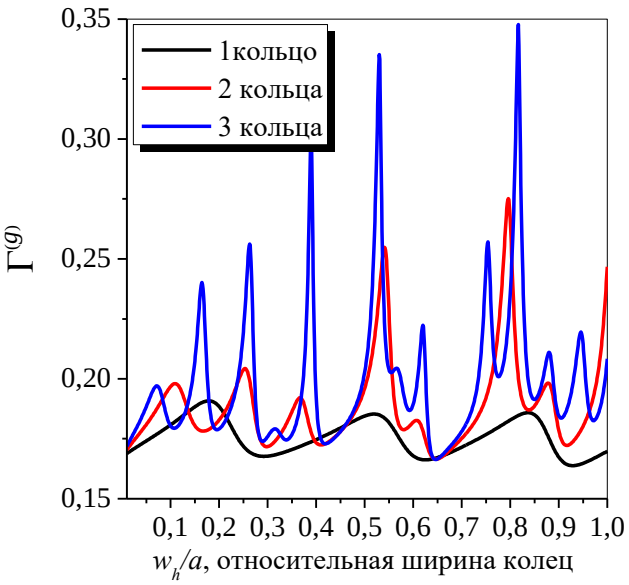

Fig. 3.25 The same as in Fig. 3.24, however for the summary overlap coefficient for the air gaps.

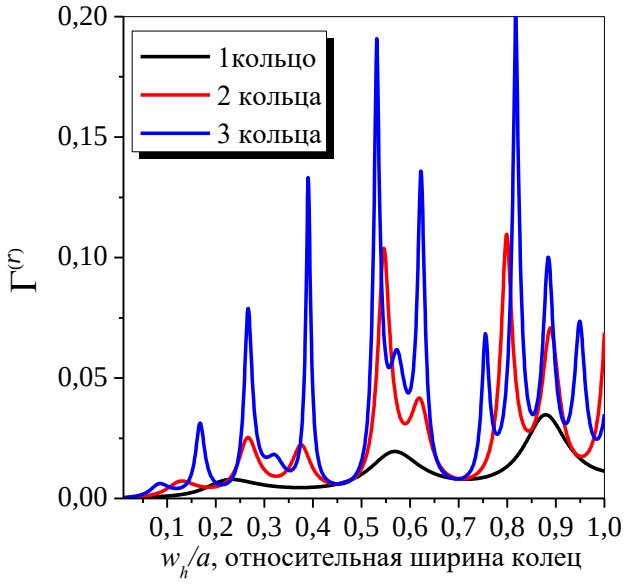

Fig. 3.26 The same as in Fig. 3.24, however for the summary overlap coefficient for the passive dielectric rings

Thus, if the thickness of the ABR rings is not small then the supermode field may be pulled into ABR and become concentrated either in the dielectric rings or in the air gaps.

CONCLUSIONS FOR CHAPTER 3

In this Chapter, we have considered the 2-D models of open circular dielectric active resonators embedded into annular reflectors made of finite number of passive dielectric rings separated with air gaps. In particular, these models have enabled us to investigate, using the lasing eigenvalue problems, the lasing frequencies and thresholds for the natural modes of a microdisk laser inside an annual Bragg reflector. The results of these studies have been published in the journal paper [6] and conference proceedings [31–33,35-39,41] and led to the following conclusions:

1. The natural modes of an active disk resonator inside a passive reflector are always “supermodes”, i.e. optically coupled modes of the partial regions: central disk resonator, rings, and air gaps. Therefore their detail description requires so many integer indices as many partial regions are in the considered configuration.

2. Any supermode of an active resonator with reflector (both the whispering gallery modes and the lower-azimuth-index modes) can have their thresholds of lasing both higher and lower than the corresponding thresholds of the same modes in the stand-alone resonator. The values of the thresholds depend on the reflector composition and the distance to its first ring.

3. The lowering of the threshold is always linked to the electric-field of the supermode pulling into the active central resonator, and the growth of the threshold is linked to the field pushing out of the active region and its pulling into the rings of reflector.

4. For the active resonator embedded into an annual Bragg reflector made of GaAs with the gaps filled with air, the adding of new ring lowers the threshold of any supermode by approximately an order of magnitude.

5. The Optical Theorem, applied to the natural mode field in an active open resonator, leads to an identity that has the meaning of the power balance equation for a laser (loss = gain). It can be used for a test of validity of obtained numerical results.

6. The mentioned above identity enables one to reach a conclusion that, in order to have low threshold of lasing, a mode on an open resonator should have not only a high Q-factor (in the absence of pumping) but also a good overlap of its electric field with the active region (under pumping). To quantify this observation, it is convenient to introduce into consideration the effective mode volume and the overlap coefficients of the partial domains (including the active region) with the electric field of each mode.

7. The behavior of the thresholds of lasing of the low-threshold supermodes as a function of the reflector parameters repeats, in general, the behavior of the inverse value of the overlap coefficient of the active region with the mode field. This is in good agreement with the Optical Theorem for lasers.